PCCP

Accepted Manuscript

ROYAL SOCIETY OF CHEMISTRY

www.rsc.org/pccp

Journal Name

ARTICLE TYPE

Cite this: DOI: 10.1039/xxxxxxxxxx

Femtosecond predissociation dynamics of the methyl radical from the $3p_z$ Rydberg state

Garikoitz Balerdi,[a] Joanne Woodhouse,[a‡] Alexander Zanchet,[b] Rebeca de Nalda,[c] María L. Senent[d], Alberto García Vela[b] and Luis Bañares[a*]

Received Date
Accepted Date

DOI: 10.1039/xxxxxxxxxx

www.rsc.org/journalname

The real time dynamics of electronic predissociation of the CH_3 radical (and its deuterated variant CD_3) from selected vibrational states of the $3p_z$ Rydberg state have been measured for the first time using a novel methodology based on a femtosecond three-color experiment to generate, two-photon excite and ionize methyl radicals as a function of time in combination with velocity map imaging detection. Subpicosecond lifetimes have been measured, showing a decreasing trend as vibrational excitation in the symmetric stretch and bending umbrella modes increases for both species. High-level *ab initio* calculations have been carried out in order to elucidate the CH_3 $3p_z$ predissociation mechanism and support the lifetime measurements. The observed lifetimes are relevant for the understanding of the resonance enhanced multiphoton ionization spectroscopy of this radical.

Introduction

The relevance of the methyl radical spans across both applied and fundamental areas of Chemistry. It is of great importance in processes like hydrocabon combustion[1], formation of complex hydrocarbons in the interstellar medium[2], troposphere chemistry[3] and chemical vapour deposition for diamond growth. Also, historically, as the simplest alkyl radical, it has been considered as a benchmark system in molecular orbital theory for the photochemistry of larger open-shell hydrocarbons. Still, some key questions relating to its spectroscopy and dynamics remain unanswered.

A crucial finding of Herzberg's seminal spectroscopic work[4], is that the methyl radical is planar and, as a consequence, many excited states cannot be observed by one-photon spectroscopy, since one-photon transitions from the ground state are forbidden. It was not until multiphoton spectroscopy was made possible with intense lasers that the new techniques, especially resonance enhanced multiphoton ionization (REMPI), enabled the acquisition of new information on excited states[5], which are the result of exciting the unpaired electron from an orbital with carbon $2p_z$ character into carbon-based orbitals with mostly Rydberg character. Out of the two-photon transitions of the methyl radical, the $3p_z$ and $4p_z$ states, in particular, have become widely used for detection of the methyl radical in the gas-phase (see, for instance, refs[6–11] among others), but it was soon realized that the acquisition of highly resolved rovibrational data was not possible due to the rapid predissociation of all excited states, particularly in the undeuterated species. The state-dependent predissociation rates also precludes obtaining quantitative data on product state distributions in reactions where CH_3 is formed, and it is for this reasons that direct comparisons have only been possible through transitions that share a common vibronic intermediate[12].

The predissociation process of the vibrational levels of the $3p_z$ state of the methyl radical has been the subject of some studies, mainly aimed at quantifying its effect on their relative REMPI detection sensitivities, which would allow the measurement of the state distribution of the methyl radical formed in reactions of the type $F + CH_4 \rightarrow CH_3 + HF$[13,14]. In ref[13] the method employed consisted of the application of a kinetic model to characterize the (2+1) REMPI process in CD_3 through the $3p_z$ state. From fits to power dependences obtained for each band, upper bounds for the predissociation rate of each state were estimated. This yielded an upper limit of 3 ps for the vibrational ground state, and this value decreased with increasing excitation in the umbrella mode, ν_2 (1 ps for ν_2=1, 0.8 ps for ν_2=2 and 0.4 ps for ν_2=3). From later work based on IR-UV double resonance[14], a 5 cm^{-1} linewidth was observed for all single rovibronic transitions of the CH_3 radical, with which an estimated lifetime of ∼1 ps can then be inferred for the ν=0 level and the symmetric stretch C-H mode ν_1=1 level.

[a] Departamento de Química Física, Facultad de Ciencias Químicas, Universidad Complutense de Madrid (Unidad Asociada I+D+i CSIC), 28040 Madrid, Spain; E-mail: lbanares@ucm.es
[b] Instituto de Física Fundamental, CSIC, C/ Serrano, 123, 28006 Madrid, Spain
[c] Instituto de Química Física Rocasolano, CSIC, C/ Serrano, 119, 28006 Madrid, Spain
[d] Departamento de Química y Física Teóricas, Instituto de Estructura de la Materia, CSIC, Serrano 121, Madrid 28006, Spain
‡ Present address: Department of Chemistry, University College London, 20 Gordon Street, London WC1H 0AJ, UK

The work of Black and Powis[8] investigated the predissociation dynamics of CH_3 and CD_3 in the $4p_z$ Rydberg state in two ways: through rotationally dependent lifetime broadened linewidths of the (2+1) REMPI spectrum and through a modified band profile due to a reduction of the ionization yield by competing predissociation of the resonant intermediate. They found an important distinction between the behavior of CH_3 and CD_3 for the predissociation mechanism in the $4p_z$ state. While for CD_3 the evidence pointed only to homogeneous predissociation, for CH_3 the authors found a significant rotational level dependence of the measured linewidths in the (2+1) REMPI spectrum, indicating that, along with the homogeneous mechanism, a heterogeneous predissociation channel was active, which was attributed to a perpendicular Coriolis coupling. From a comparison of experimental and simulated (2+1) REMPI spectra, the authors proposed that an analogous situation should apply, at least qualitatively, for predissociation from the $3p_z$ Rydberg state. The authors also suggested a candidate state ($3d\ ^2E''$) whose interaction with the $4p_z$ Rydberg state could be responsible for the homogeneous predissociation.

The rovibrational dependence of predissociation rate of the $3s$ Rydberg state of the methyl radical was investigated by resonance enhanced Raman spectroscopy by Westre *et al.*[15,16] and in this state the lifetime of CD_3 was found to halve upon with one quantum of excitation in the umbrella mode, ν_2. In ref[16], rotation-dependent subpicosecond lifetimes were obtained with a smooth J dependence. Later on, the photodissociation dynamics of CH_3 from the $3s$ Rydberg state at 193.3 nm was studied using photofragment translational spectroscopy[17]. Only CH_2 and $H(^2S)$ fragments were observed and although it was not possible to assign the spin state of CH_2 unambiguously, it was suggested that it was produced predominately in the $\tilde{a}\ ^1A_1$ excited state. The measured translational energy distribution of the products was consistent with the presence of an exit barrier on the $3s$ potential energy surface and an anisotropy parameter of β=–0.9±0.1 was determined corresponding to a perpendicular transition. Yang and co-workers[18,19] studied the photodissociation of CH_3 from the $3s$ Rydberg state at 212.5 nm using the H-atom Rydberg tagging time-of-flight technique with a pure CH_3 radical source generated by photolysis of CH_3I at 266 nm. Time-of-flight spectra of the H-atom products from the photolysis of both cold and hot CH_3 radicals were measured at different photolysis polarizations. The experimental results indicated that the photodissociation of the CH_3 radical in its ground vibrational state occurs on a very fast time scale in comparison with its rotational period. Experimental evidence also shows that photodissociation in the ν_2=1 vibrational state of the umbrella mode is characteristically different from that in the ground vibrational state.

Theoretical studies on the predissociation dynamics of the methyl radical are very scarce[16,20,21] In the work of Yu *et al.*[20], a small basis set RHF calculation was performed to obtain semi-quantitative information about the relative barrier heights of radical ($CH_3 \rightarrow CH_2$ + H) and molecular ($CH_3 \rightarrow CH + H_2$) predissociation pathways from the ground, $3s$ and $3p$ states of the methyl radical. The group also used calculated relative energies of products and concluded that at the excitation energy of the $3p_z$ state, it is thermodynamically possible to form the $\tilde{X}\ ^3B_1$, $1\ ^1A_1$, $1\ ^1B_1$ and $2\ ^1A_1$ states of CH_2 as the product of radical predissociation, and $CH(A\ ^2\Delta)$ and $CH(X)$ as products of molecular predissociation. However, based upon orbital correlations it was predicted that the dominant reaction pathway for predissociation from the $3p_z$ state would be radical predissociation forming $CH_2(1\ ^1B_1)$+H. This calculation predicted a much larger reaction barrier for radical predissociation at planar geometry from the $3p_z$ state than from the $3s$ state, which is in agreement with the higher resolution observed in REMPI spectra via the $3p_z$ state.

It is known that lifetimes extracted from spectral linewidths or indirect methods may have large errors due to competing experimental broadening effects which are difficult to quantify (*e.g.* Doppler and pressure broadening effects), and that the use of an appropriate femtosecond pump-probe scheme allows for direct extraction of the time constant for the population decay of predissociative electronic excited states[22–24]. The method involves using the short pump pulse to excite the molecule to the vibronic state of interest and the probe pulse to ionize the state population after a variable delay.

In this work, we report the first direct, real-time measurements of the lifetimes of selected vibrational levels of the $3p_z$ Rydberg state of CH_3 and its deuterated form CD_3. In addition, high-level *ab initio* calculations of the electronic states involved in the $CH_3 \rightarrow CH_2$ + H radical dissociation process have been carried out with the aim of interpreting and rationalizing the experimental findings. The resulting interpretation along with the accurate lifetime measurements obtained provide valuable information about one of the main dissociation pathways of this important radical system.

In contrast to more commonly used methods for CH_3 synthesis like pyrolisis of a suitable precursor[17] or A-band photodissociation of CH_3I[18,19], the method chosen for the generation of CH_3 (CD_3) radicals has been B-band photodissociation of CH_3I (CD_3I). The high cross section for this process in the precursor CH_3I (CD_3I) molecule ($\sigma \approx 600\times10^{-18}$ cm^2 at 201.2 nm, the band origin[25]) guarantees a high density of CH_3 radicals in the interaction region. Electronic predissociation in the precursor occurs via the route $I^*(^2P_{1/2})$ + $CH_3(v)$, the methyl fragment appearing in the ground electronic state and in a broad distribution of vibrational levels[23]. The experiment is then realized according to the scheme shown in Figure 1, analogous to the scheme employed in ref[26] for NH_3. A short pulse tuneable in the region of 330 nm (two-photon resonant with the $3p_z\ ^2A_2'' \leftarrow \tilde{X}\ ^2A_2''$ transition) is used to transfer population to the $3p_z$ Rydberg state. A delayed pulse centered at 400 nm interacts with the excited sample, causing ionization. Methyl ions are detected as a function of the delay between the excitation (330 nm) and ionization (400 nm) pulses. As indicated in Figure 1, the (2+1) REMPI (one-color) process coexists with the (2+1′) (two-color) process, and thus it is necessary to subtract the methyl ion signal caused by the excitation pulse alone to obtain transients like that sketched in the Figure, from where the lifetimes can be readily obtained. By using a combination of vibrationally selective excitation and kinetic energy information provided by velocity map imaging (VMI) detection of methyl fragments, lifetimes of the $3p_z$ state of the methyl radical have been

measured with specificity in the ν_1 and ν_2 vibrational modes, as we will show below.

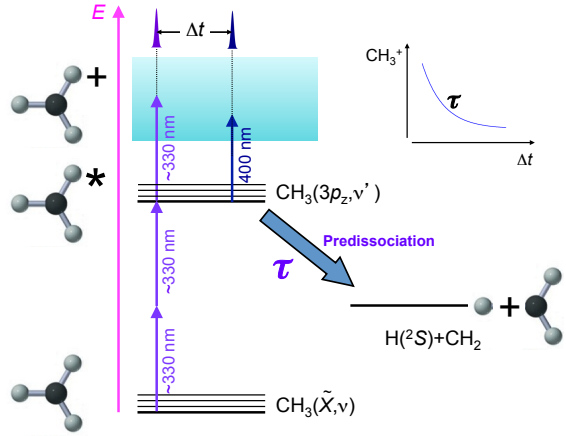

Fig. 1 Scheme of the experimental procedure to obtain lifetimes of the $3p_z$ vibrational levels in CH_3. A short, tuneable laser pulse centered around 330 nm (two-photon resonant with the $3p_z\ ^2A_2'' \leftarrow \tilde{X}\ ^2A_2''$ transition in CH_3), is used for excitation. A short pulse of 400 nm, delayed by Δt, probes the surviving population in the $3p_z$ Rydberg state by causing ionization, producing a signal that is proportional to the instantaneous population in the Rydberg state, schematically shown in the inset.

Methods

Experimental

The laser was an amplified Spectra Physics Ti:Sapphire system which delivers 50 fs pulses centered at 805 nm with an average pulse energy of 3.5 mJ and a repetition rate of 1 kHz. The output was split into three separate beams. The first beam was used for triggering the UV photodissociation of CH_3I (or CD_3I) as precursor of the CH_3 (CD_3) radicals under study. The UV laser light was generated through frequency quadrupling of the fundamental, which passed through a frequency tripling unit followed by a sum-frequency mixing unit. This was tuned to 201.2 nm for the 0_0^0 transition of the B-band in CH_3I (or 200.5 nm in CD_3I). The full width at half maximum (FWHM) bandwidth of the 201.2 nm beam was 0.3 nm, and the average pulse energy was below 1 μJ. Absorption is followed by predissociation yielding CH_3 (or CD_3) in a range of vibrational states. The second beam was passed through an optical parametric amplifier (OPA) which produced tunable light in the region of 1.2-1.3 μm, which is then frequency quadrupled to synthesize wavelengths at around 330 nm for two-photon excitation of methyl radicals into the $3p_z$ Rydberg state. The FWHM bandwidth of this arm is 2.5 nm, allowing vibrational selectivity in this step. The third part of the 804 nm fundamental beam was frequency doubled to produce pulses centered at 402 nm with average pulse energy <3 μJ, which is sufficient for one-photon ionization of the $3p_z$ state of the methyl radical. The polarization of all three pulses was horizontal and parallel to the face of the ion detector. The relative arrival times of the pulses were controlled with two mechanical delay stages with time resolution of 1 fs, in the 330 nm and 400 nm arms. The position of the focal plane of the 200 nm and 400 nm beams was controlled using telescopes. The three beams were coupled collinearly into the vacuum chamber through a 25 cm focal length lens. The instrument temporal response was taken to be equal to the cross correlation of the 330 nm and 400 nm pulses, which was measured through multiphoton ionization of Xe to be 140 fs. The time delay between the 201.2 nm (or 200.5 nm) beam and the other beams, causing CH_3I dissociation, is not an important parameter, and it is simply fixed at a value that is sufficiently long so that the predissociation process is completed (30 ps).

CH_3I (or CD_3I), kept at 0°C and seeded in He at a total pressure of 1.5 bar, was expanded into vacuum through a homemade 1 kHz piezoelectric pulsed valve with a 0.5 mm nozzle diameter. The molecular beam then passes through a skimmer which separates the source chamber from the ionization chamber. The ions formed in the interaction region are extracted perpendicularly by a set of open electrodes in velocity mapping configuration[27], permitting 100% transmittance and detector-spot limited velocity resolution. The detector is situated at the end of a 50 cm time-of-flight (TOF) tube and consists of a pair of microchannel plates, in Chevron configuration, coupled to a phosphor screen. Typical repeller voltages were 5200 V for CH_3^+ imaging and 4500 V for CD_3^+ imaging, with optimal velocity mapping conditions found for $V_{\text{extractor}}/V_{\text{repeller}}=0.76$. Mass selection is achieved by gating the gain of the front MCP plate. The phosphorescence is recorded on a Peltier-cooled 12 bit charge-coupled device camera. Typical image acquisition times were set at 800 ms, corresponding to 800 laser shots. The contribution of dissociative ionization was removed by subtracting the image obtained in the presence of 200 nm alone from the images obtained in the presence of all three laser beams. The images were inverted using the polar basis set expansion (pBasex) method.[28] The velocity calibration of images was carried out using the the known kinetic energy of nascent $CH_3(v=0)$ following 201.2 nm photodissociation of methyl iodide, which proceeds via the $CH_3+I^*(^2P_{1/2})$ product channel, and (2+1) resonant multiphoton ionization at 333.45 nm.

Theoretical

Electronic structure computations of geometries and electronic states of CH_3 have been carried out using MOLPRO[29]. At the ground electronic state, the methyl radical is a planar molecule of D_{3h} symmetry. Since D_{3h} is not an Abelian group, all *ab initio* calculations were performed using the C_{2v} group representation, which is valid as long as the molecule remains in a planar configuration. In order to calculate the dissociation of the CH_3 radical along the C–H distance, geometry optimization in the ground state of CH_3 was carried out at different C–H distances using the complete active space self-consistent field (CASSCF) method[30,31] followed by the multireference perturbation theory CASPT2 method[32]. In all cases, the augmented correlation consistent basis set (aug-cc-pVTZ)[33] was employed.

Using the optimized geometries, the ground and excited electronic state energies were computed using CASSCF followed by the internally contracted multi reference configuration interaction (MRCI)[34] approach. The orbitals included in the active

space are (3-10)a_1, (1-4)b_1, and (1-3)b_2, while the $1a_1$ and $2a_1$ molecular orbitals (associated to the $1s$ and $2s$ orbitals of the carbon atom) were considered to be doubly occupied in all configurations. For the MRCI calculations the $1s$ orbital was kept frozen. Calculations were restricted to the four first states of A_1 and four first states of B_1 symmetries in C_{2v}. To establish the valence/Rydberg character of the states, the spatial extent was estimated through the computation of the quadrupolar moments. A threshold value of 40 a.u. was established for the valence/Rydberg distinction.

The obtained adiabatic potential energy curves have been diabatized for a more appropriate interpretation in terms of the dissociation of the radical along the C–H distance. For both A_1 and B_1 symmetry representations, we have applied a 3×3 diabatization model to get the diabatic potential energy curves and their diabatic electronic couplings for each symmetry. Considering three adiabatic states a_1, a_2 and a_3, we generate three diabatic states d_1, d_2 and d_3 following a sequential 2×2 diabatization scheme based on energy criteria. The assumptions made are, (a) if two states cross each other, they do it only once (valid in the present case); (b) total energy is conserved (*i.e.*, $a_i + a_j = d_i + d_j$); (c) outside the interaction region $\boldsymbol{I}$, diabatic potential energy curves match the adiabatic ones. $\boldsymbol{I}$ is defined as the region where $\Delta E < \Delta E_{min} + \xi$, where ΔE represents the energy difference between the two adiabatic states considered, ΔE_{min} is the minimum energy difference between them, and ξ is an arbitrary threshold to adapt in each case. Following those constraints, the d_i state is constructed by linking the left part of a_i and the right part of a_j by interpolation in the $\boldsymbol{I}$ region. The other diabatic curve is then built as $d_j = a_i + a_j - d_i$. When the two first diabatized state are obtained, the same procedure is repeated between both of them and the third adiabatic state, adapting ξ to the topology of the curves (in the present case, we considered 0.2 a.u. $< \xi <$ 0.5 a.u.).

Results and discussion

Figure 2 shows the measured methyl ion signals in the one-color experiment, *i.e.* only the pulse around 330 nm is employed in this case. The nascent CH_3 (CD_3) fragments from CH_3I photodissociation are detected via (2+1) REMPI by tuning the laser in the region of 330 nm and detecting the ions in VMI configuration. The vibronic transitions used in this experiment are the diagonal transitions corresponding to ν_2=0,1,2,3 Due to the spectral proximity of these transitions to diagonal vibronic transitions of the ν_1 mode, it has been shown before[23,24] that activity in both modes can be detected simultaneously if the laser source possesses sufficiently broad bandwidth.

Figure 2a shows a CH_3^+ Abel-inverted image obtained under these conditions, where the excitation laser is tuned to a centre wavelength of 333.5 nm, resonant with the 0_0^0 vibronic band of the $3p_z\ ^2A_2'' \leftarrow \tilde{X}\ ^2A_2''$ transition. Together with the main ring, a dimmer ring appears, with lower radius, *i.e.*, lower kinetic energy; it corresponds to the 1_1^1 vibronic band of the $3p_z\ ^2A_2'' \leftarrow \tilde{X}\ ^2A_2''$ transition, that can be detected due to the broadband character of the 333.5 nm laser[23]. Kinetic energy distributions obtained from this image and those corresponding to excitation of the 2_1^1 and 2_2^2 vibronic bands, for which the excitation laser is retuned to 329.4 nm and 325.8 nm, respectively, are shown in Figure 2b. The state distribution observed here for CH_3 produced by predissociation of CH_3I via the vibrational ground state of the $^3R_1$ Rydberg state includes ν_2=0,1,2 with ν_1=0,1, in agreement with that observed by Gitzinger *et al.*[23]

The analogous measurement for the case of CD_3 resulting from predissociation of CD_3I at 200.5 (origin of the B-band), with (2+1) REMPI of CD_3 at 333.8 nm (resonant with the 0_0^0 vibronic band of the $3p_z\ ^2A_2'' \leftarrow \tilde{X}\ ^2A_2''$ transition) yields the Abel-inverted image of CD_3^+ shown in Figure 2c. Although the image may seem similar to that of CH_3^+ in Figure 2a, careful inspection indicates that the main ring does not correspond to the 0_0^0 transition, as it did for CH_3, but instead, it corresponds to 1_1^1, and the dimmer, internal ring, to the 1_2^2 transition. The complete set of kinetic energy distributions is shown in Figure 2d. As can be seen, there is a marked vibrational population inversion in CD_3 as compared with CH_3, to the point that no CD_3 is formed in the ν_1=0,ν_2=0 vibrational state. This implies that lifetime measurements have not been possible for the vibrationless ν=0 level of CD_3.

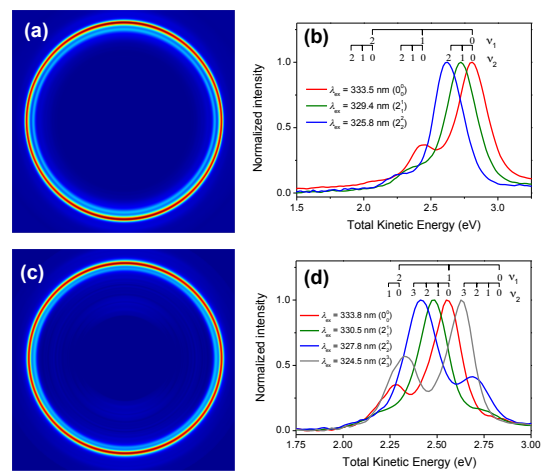

Fig. 2 Results of the (2+1) REMPI experiment of nascent CH_3 (CD_3) after B-band photodissociation of CH_3I (CD_3I). (a) Abel-inverted velocity map image of CH_3^+ obtained at 333.5 nm. (b) Total kinetic energy distributions obtained from angular integration of Abel-inverted images at 333.5 nm (red, 0_0^0 transition), 329.4 nm (green, 2_1^1 transition) and 325.8 nm (blue, 2_2^2 transition). (c) Abel-inverted velocity map image of CD_3^+ obtained at 333.8 nm. (d) Total kinetic energy distributions obtained from angular integration of Abel-inverted images at 333.8 nm (red, 0_0^0 transition), 330.5 nm (green, 2_1^1 transition), 327.8 nm (blue, 2_2^2 transition) and 324.5 nm (grey, 2_3^3 transition). Transitions wavelengths from ref[35].

For the lifetime measurements, the third laser pulse at 400 nm was added after a controlled delay time. The methyl ion images were qualitatively analogous to those obtained with one-color REMPI, but signal levels were higher in a time window of a few hundreds of femtoseconds. An example of the kinetic energy distributions obtained for each pump-probe delay time is shown in

Figure 3a in the form of a false color map for the case of CH_3 at 333.5 nm (0_0^0 and 1_1^1 vibronic transitions). The two visible channels correspond, therefore, as in Figure 2a, to the v=0 and v_1=1 levels. Since CH_3^+ signals thus measured are a result of both the (2+1′) and (2+1) REMPI processes, subtraction of the images obtained under 333.5-nm-only irradiation was necessary to isolate the (2+1′) processes that yielded information of lifetimes. The result of such subtraction is shown in Figure 3b. Interestingly, no signal was observed in the (2+1) and (2+1') experiments when the excitation laser was detuned from resonance.

A two-dimensional nonlinear least squares fit to the maps was performed using the Levenberg-Marquardt algorithm following the procedure described in ref[24]. Each peak in the kinetic energy distribution was fit with a Gaussian function in the energy dimension such that the lifetimes of the individual states could be measured independently. The variation of the amplitude of these Gaussian functions with delay time was fit with an exponential decay convoluted with another Gaussian function to account for the instrument response. A third Gaussian contribution was also employed, centered at the temporal overlap of the two pulses, t_0, to describe two-color multiphoton ionization processes that may occur upon simultaneous absorption. The decrease in signal intensity observed with increasing delay was attributed to the population decay due to predissociation of the intermediate $3p_z$ state. Transients obtained for the two channels visible in the maps in Figure 3b are shown in Figures 3c and 3c3d. Single exponential functions were proven to reproduce the time-varying signal levels within experimental error, and thus the time constants obtained from the fits for each of the channels are assigned to the lifetimes of each vibrational level.

As was the case for the detection of the nascent CH_3 (CD_3) populations through (2+1) REMPI, measurement of the lifetimes of as many vibrational levels as possible required retuning the excitation laser to achieve population transfer to a broad set of (v_1,v_2) levels. Table 1 contains the results of the complete set of measurements for the $3p_z$ state of CH_3 and CD_3.

Table 1 Measured lifetimes (τ) values (in fs) of the vibrational levels of the $3p_z$ state of the CH_3 and CD_3 radicals.

v_1	v_2	CH_3, τ (fs)	CD_3, τ (fs)
0	0	720 ± 70	–
0	1	500 ± 50	1200 ± 100
0	2	320 ± 100	1400 ± 100
0	3	–	830 ± 80
1	0	410 ± 70	1200 ± 200
1	1	310 ± 90	800 ± 30
1	2	300 ± 40	600 ± 40
1	3	–	390 ± 20
2	0	–	520 ± 80
2	1	–	500 ± 100

It is somewhat unexpected that single exponential functions are capable of describing the temporal decays with sufficient accuracy. In principle, given that several transitions to a broad set of rotational levels can be coherently excited by the ultrashort pulses, contributing to the global ionization signal, multiexponential decays could be expected. In the analogous experiment by Dobber *et al.* in ammonia[26], the authors found that biexponential decay functions were necessary to fit the observed decays for most vibrational levels. They attributed this result to different lifetimes of the low-lying versus the high-lying rotational levels. In our case, the fact that single exponential functions are always sufficient to obtain good fits to the data points to a mild rotational dependence of the lifetimes. The implication of this weak rotational dependence is a higher accuracy of the lifetimes obtained from the transients.

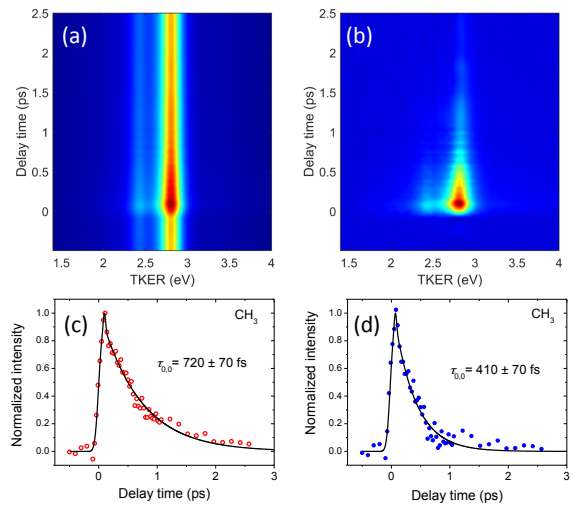

Fig. 3 Measurement of vibrational state-dependent lifetimes of vibrational levels of the $3p_z$ Rydberg state in CH_3. (a) False color map representing the total kinetic energy distributions, obtained from Abel-inverted images, under two-color irradiation (333.5 nm + 400 nm) as a function of the delay time between the laser pulses. Two channels are visible, the main one corresponding to the 0_0^0 transition, and the weaker, lower kinetic energy channel, to the 1_1^1 transition. (b) Same as (a), but after subtraction of the single color, 333.5 nm contribution. (c) Transient of the channel corresponding to the 0_0^0 transition (revealing remaining population in v=0, obtained from the map shown in (b)). A lifetime of 720±70 fs is obtained for the v=0 level of the $3p_z$ Rydberg state in CH_3. (d) Transient of the channel corresponding to the 1_1^1 transition (revealing remaining population in v_1=1, obtained from the map shown in (b)). A lifetime of 410±70 fs is obtained for the v_1=1 level of the $3p_z$ Rydberg state in CH_3.

Lifetimes reported in Table 1 have been represented in graphic format in Figure 4 for both CH_3 and CD_3 as a function of the energy of the level under consideration above the v=0 level. For CH_3, it was known that the 0_0^0 vibronic transition was the only one where rotational structure could be resolved[5], consistently with the longest value found here for the predissociation lifetime of the v=0 level. The isotopic effect that favors rapid predissociation for the undeuteraded species is clear from the graph, lifetimes measured for CD_3 being more than twice as long as for CH_3 for all cases. Also, a rather monotonic trend is observed as a function of energy which seems irrespective of the vibrational mode or mode combination under consideration.

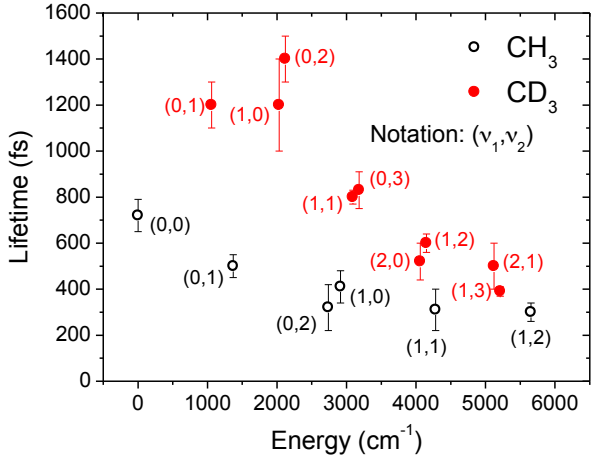

Fig. 4 Measured lifetimes of a set of (v_1,v_2) levels of the $3p_z$ Rydberg state of CH_3 (black empty circles) and CD_3 (solid red circles), plotted as a function of vibrational excess energy above the (0,0) level.

In order to shed light into the predissociation mechanism and the measured state selected lifetimes of the methyl radical from the $3p_z$ Rydberg state, high level electronic structure *ab initio* calculations have been performed for the CH_3 and CH_2 radicals. As commented on above, *ab initio* calculations for electronically excited states of the CH_3 radical reported in the literature are very scarce due to the difficulties inherent to its open shell character. In the following, we present the first high-level MRCI calculations of excited states (up to energies of about 12 eV) which are involved in the photochemistry of CH_3. In Table 2, the vertical excitation energies (VEE) from the ground state equilibrium geometry to the excited electronic states of A_1 and B_1 symmetries in C_{2v} for CH_3 are summarized and compared with the available previous calculations and experimental data. The VEE to the different electronic excited states of CH_2 are also shown in the Table. As can be seen, the correlation between the calculated VEE and the available experimental transitions is quite reasonable.

Ab initio potential energy curves as a function of the C–H distance have been calculated for the most relevant electronic states involved in the predissociation dynamics of CH_3 from the $3p_z\ ^2A_2''$ Rydberg state. Considering the large number of electronic states for CH_3 and that adiabatic curves are not easy to follow, all C_{2v} A_1 and B_1 states of interest have been diabatized following a three-state diabatic model to take into account the non-adiabatic interactions between electronic states, and the resulting curves are depicted in Figure 5. The ground electronic state of CH_3 in D_{3h} symmetry, $\tilde{X}\ ^2A_2''$, is a non-degenerate doublet. Considering the *ab initio* VEE values shown in Table 2, the first excited state of CH_3 is $3s\ ^2A_1'$, which presents a strong Rydberg character and lies 5.84 eV over the ground state. At around 7 eV, two states are observed, one associated with a $3p_{x,y}\ ^2E'$ Rydberg state (not characterized experimentally), which presents A_1 character in C_{2v}, and a valence dissociative state of the same symmetry, $^2E'$. This valence state interacts with the $3p_{x,y}\ ^2E'$ Rydberg state in the Franck-Condon region and also with the $3s\ ^2A_1'$ Rydberg state at a larger CH distance. Above in energy lies the $3p_z\ ^2A_2''$ Rydberg state at 7.65 eV, which is the one excited in the experiment by two-photon absorption. Finally, at around 12 eV, we find a valence dissociative state (the $4\ ^2B_1$ in C_{2v}), which crosses the $3p_z\ ^2A_2''$ Rydberg state when the C–H bond is elongated.

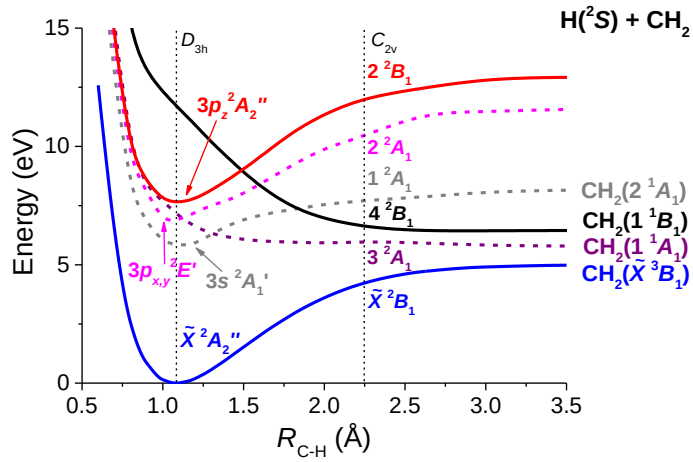

Fig. 5 Diabatic *ab initio* potential energy curves of A_1 (dashed) and B_1 (solid) symmetry in C_{2v} relevant for predissociation of the $3p_z\ ^2A_2''$ Rydberg state of the methyl radical, along the C–H coordinate.

It is important to emphasize that if the ν_2 umbrella mode is active and the radical geometry is out of the planar configuration, then the D_{3h}/C_{2v} symmetry will brake down to C_{3v}/C_s. This can alter the dissociation mechanism quite significantly, since the A_1 and B_1 representations in the C_{2v} symmetry group will both correlate to A' in C_s (A_2'' and A_1' in D_{3h} correlate to A_1 in C_{3v}). In that case, all states shown in Figure 5 will couple together.

Consequently, dissociation can follow several competing mechanisms. The fastest one is expected to be the direct predissociation from the $3p_z\ ^2A_2''$ Rydberg state to the valence dissociative $4\ ^2B_1$ state (see Figure 5). This state leads to CH_2 in the excited $1\ ^1B_1$ state. Since the crossing occurs at an elongated C–H distance of about 1.5 Å, the C–H stretch vibrational mode excitation in CH_3 would favor this mechanism, as confirmed by the shorter observed lifetimes when the ν_1 mode excitation increases. This $4\ ^2B_1$ valence state also crosses the two lower $3s\ ^2A_1'$ and $3p_{x,y}\ ^2E'$ Rydberg states. Therefore, the system can eventually relax to these states opening new routes of dissociation yielding CH_2 in different excited states. However, these alternative mechanisms would be expected to occur at longer time scales and they are probably not seen in the present experiment where we are monitoring the time-dependent depopulation of the CH_3 radical from the initially excited $3p_z\ ^2A_2''$ Rydberg state. In addition, as none of the excited states cross the ground state, it is unlikely that internal conversion can be thought as an effective mechanism for dissociation into the ground state.

The *ab initio* calculations of the different electronic states (and their corresponding couplings) involved in the CH_3 dissociation provide a valuable tool to elucidate the specific dissociation mechanism which the measured lifetimes are associated with. Based

Table 2 MRCI vertical excitation energies (VEE) to the excited electronic states of methyl (CH_3) and methylene (CH_2).

Symmetry			CH_3		
D_{3h}	C_{2v}	Character	VEE (eV)	Prev. calc. (eV)	Expt. (eV)[36]
$\tilde{X}\ ^2A_2''$	$\tilde{X}\ ^2B_1$	Valence	0.0	0.0	0.0
$3s\ ^2A_1'$	$1\ ^2A_1$	Rydberg	5.84	5.68[20]	5.73
$3p_{x,y}\ ^2E'$	$2\ ^2A_1 + 1\ ^2B_2$	Rydberg	6.87	6.92[20]	–
$^2E'$	$3\ ^2A_1 + 2\ ^2B_2$	Valence	7.14	7.17[20]	–
$3p_z\ ^2A_2''$	$2\ ^2B_1$	Rydberg	7.65	7.19[20]	7.43
$3d\ ^2A_1'$	$4\ ^2A_1$	Rydberg	8.47	7.77[20]	8.28
	$3\ ^2B_1$	Rydberg	11.08	–	–
	$4\ ^2B_1$	Valence	11.60	–	–
	C_{2v}		CH_2		
	$\tilde{X}\ ^3B_1$		0.0	0.0	0.0
	$1\ ^1A_1$		0.98	0.48[37]	0.39
	$1\ ^1B_1$		1.48	1.54[37]	1.43
	$2\ ^1A_1$		3.16	2.67[37]	–
	$1\ ^3A_1$		6.35	–	–
	$3\ ^1A_1$		6.60	–	–
	$1\ ^3A_2$		7.34	–	–
	$2\ ^3B_1$		7.45	–	–
	$1\ ^3B_2$		7.57	–	–
	$2\ ^1B_1$		7.72	–	–
	$3\ ^3B_2$		7.93	–	–

on the *ab initio* results the following picture would be a consistent interpretation of the experimental findings of Table 1 and Figure 4. As mentioned above, the *ab initio* calculations indicate that the $3p_z\ ^2A_2''$ Rydberg state initially excited in the experiment crosses the valence dissociative $4\ ^2B_1$ state at around $R_{C-H} = 1.5$ Å (see Figure 5). In the calculations these two states are found to be coupled nonadiabatically by a nearly Gaussian shape coupling that peaks at the crossing point. Such a coupling would be the responsible for electronic predissociation from the $3p_z$ Rydberg state to the $4\ ^2B_1$ state.

The monotonic decrease of the lifetimes of both CH_3 and CD_3 found experimentally with increasing vibrational excitation (Table 1) or energy (Figure 4) can be explained as follows. The lifetime of an initially populated vibrational state ψ_{v_1,v_2} of the $3p_z$ Rydberg state (with associated vibrational energy E_{v_1,v_2}) predissociating to a continuum state $\chi_{E=E_{v_1,v_2}}$ of $4\ ^2B_1$, can be expressed as $\tau \sim 1/C$, where $C =< \psi_{v_1,v_2}|V_{coup}|\chi_{E=E_{v_1,v_2}} >$, being V_{coup} the nonadiabatic coupling between the two electronic states. A monotonic increase of the magnitude of C is what causes the decrease of τ. Since both the magnitude and position of V_{coup} are fixed, regardless the initial vibrational excitation, only changes in the shape of ψ_{v_1,v_2} and $\chi_{E=E_{v_1,v_2}}$ with increasing vibrational excitation and energy is what can cause an increase (decrease) of C (τ)[38]. Indeed, increasing the v_1 stretching excitation causes an increase of the spatial spreading of ψ_{v_1,v_2} toward larger R_{C-H} distances. Similarly, the corresponding increase of the energy $E = E_{v_1,v_2}$ causes also a larger delocalization of the continuum wave function $\chi_{E=E_{v_1,v_2}}$ toward shorter R_{C-H} distances. The result is a larger overlap between ψ_{v_1,v_2}, V_{coup}, and $\chi_{E=E_{v_1,v_2}}$, leading to a larger C value and a shorter τ. An increasing excitation of the v_2 mode has a similar effect because also contributes to a larger spatial (in the angular mode) delocalization of the wave functions, and then also leads to a larger magnitude of C. However, the effect of the angular delocalization of the wave functions is expected to be smaller than in the case of the stretching mode, and this explains the smaller effect of v_2 excitation on the lifetime found experimentally. The isotopic effect, reflected in the longer lifetimes found for CD_3, would have a similar explanation, being due to a larger spatial localization of the wave functions ψ_{v_1,v_2} and $\chi_{E=E_{v_1,v_2}}$ because of the lower energies associated with the corresponding (v_1, v_2) vibrational states caused by the larger mass of CD_3, leading to smaller (longer) values of C (τ).

The above interpretation, supported by the *ab initio* results, associates the lifetimes measured with a direct predissociation process between the $3p_z\ ^2A_2''$ and $4\ ^2B_1$ electronic states induced by a nonadiabatic coupling. This interpretation therefore precludes the possibility (that one might consider) of dissociation by tunneling through a barrier between the two states. First, the typically subpicosecond lifetimes found experimentally for CH_3, and more remarkably also for CD_3, are clearly inconsistent with a slow tunneling mechamism. Second, the existence of a nonadiabatic coupling predicted by the *ab initio* simulations provides strong theoretical support to the direct predissociation mechanism.

Conclusions

Accurate subpicosecond lifetimes have been determined for selected vibrational states of the $3p_z$ Rydberg state of the methyl radical using a three-color femtosecond laser experiment in combination with ion imaging techniques. A clear isotopic effect (lifetimes are longer by a factor of about two for the deuterated species) is observed. Vibrational excitation (in the stretching and bending modes) produces a monotonic decrease of the lifetime. The high-level *ab initio* calculations carried out in this work help to rationalize the dynamics in terms of an electronic predissociation process induced by a nonadiabatic coupling between Rydberg

and valence excited states. It is envisioned a strong impact of the present study for the understanding of the resonance enhanced multiphoton ionization spectroscopy of this relevant radical.

Acknowledgements

This work has been financed by the Spanish Ministry of Economy and Competitiveness (MINECO) through grants CTQ2012-37404-C02-01, CTQ2012-36184, FIS2011-29596-C02-01 and FIS2013-40626-P and EU through the COST Actions Grant Nos. CM1401 and CM1405. This research was performed within the Unidad Asociada Química Física Molecular between Departamento de Química Física of Universidad Complutense de Madrid (UCM) and Consejo Superior de Investigaciones Científicas (CSIC). The facilities provided by the Centro de Asistencia a la Investigación de Láseres Ultrarrápidos at UCM are acknowledged. The Centro de Supercomputación de Galicia (CESGA, Spain) and CTI (CSIC) are acknowledged for the use of their resources.

References

1 K. C. Smyth and P. H. Taylor, *Chem. Phys. Lett.*, 1985, **122**, 518.
2 H. Feuchtgruber, F. P. Helmich, E. F. van Dishoeck and C. M. Wright, *Astrophys. J.*, 2000, **535**, L111.
3 R. P. Wayne, *Chemistry of Atmospheres*, Oxford University Press, Oxford, 2000.
4 G. Herzberg, *Proc. R. Soc. A Math. Phys. Eng. Sci.*, 1961, **262**, 291.
5 J. W. Hudgens, T. G. DiGuiseppe and M. C. Lin, *J. Chem. Phys.*, 1983, **79**, 571.
6 J. M. Jasinski, B. S. Meyerson and B. A. Scott, *Annu. Rev. Phys. Chem.*, 1987, **38**, 109.
7 D. H. Parker, Z. W. Wang, M. H. M. Janssen and D. W. Chandler, *J. Chem. Phys.*, 1989, **90**, 60.
8 J. F. Black and I. Powis, *J. Chem. Phys*, 1988, **89**, 3986.
9 I. Powis and J. F. Black, *J. Phys. Chem.*, 1989, **93**, 2461.
10 B. Martínez-Haya, I. Zapater, P. Quintana, M. Menéndez, E. Verdasco, J. Santamaría, L. Bañares and F. J. Aoiz, *Chem. Phys. Lett.*, 1999, **311**, 159.
11 P. Quintana, R. F. Delmdahl, D. H. Parker, B. Martínez-Haya, F. J. Aoiz, L. Bañares and E. Verdasco, *Chem. Phys. Lett.*, 2000, **325**, 146.
12 R. O. Loo, H.-P. Haerri, G. E. Hall and P. L. Houston, *J. Chem. Phys.*, 1989, **90**, 4222.
13 J. Zhou, J. J. Lin, W. Shiu, S.-C. Pu and K. Liu, *J. Chem. Phys.*, 2003, **119**, 2538.
14 W. Zhang, H. Kawamata, A. J. Merer and K. Liu, *J. Phys. Chem. A*, 2009, **113**, 13133.
15 S. G. Westre, P. B. Kelly, Y. P. Zhang and L. D. Ziegler, *J. Chem. Phys.*, 1991, **94**, 270.
16 S. G. Westre, T. E. Gansberg, P. B. Kelly and L. D. Ziegler, *J. Phys. Chem.*, 1992, **96**, 3610.
17 S. W. North, D. A. Blank, P. M. Chu and Y. T. Lee, *J. Chem. Phys.*, 1995, **102**, 792.
18 G. Wu, B. Jiang, Q. Ran, J. Zhang, S. A. Harich and X. Yang, *J. Chem. Phys.*, 2004, **120**, 2193.
19 G. Wu, J. Zhang, S. A. Harich and X. Yang, *Chin. J. Chem. Phys.*, 2006, **19**, 109.
20 H. T. Yu, A. Sevin, E. Kassab and E. M. Evleth, *J. Chem. Phys.*, 1984, **80**, 2049.
21 P. Botschwina, E. Schick and M. Horn, *J. Chem. Phys.*, 1993, **98**, 9215.
22 A. P. Baronavski and J. C. Owrutsky, *J. Chem. Phys.*, 1998, **108**, 3445.
23 G. Gitzinger, M. E. Corrales, V. Loriot, G. A. Amaral, R. de Nalda and L. Bañares, *J. Chem. Phys.*, 2010, **132**, 234313.
24 G. Gitzinger, M. E. Corrales, V. Loriot, R. de Nalda and L. Bañares, *J. Chem. Phys.*, 2012, **136**, 074303.
25 S. Eden, P. Limao-Vieira, S. V. Hoffmann and N. J. Mason, *Chem. Phys.*, 2007, **331**, 232.
26 M. R. Dobber, W. J. Buma and C. A. de Lange, *J. Phys. Chem.*, 1995, **99**, 1671.
27 A. T. Eppink and D. H. Parker, *Rev. Sci. Instrum.*, 1997, **68**, 3477.
28 G. A. García, L. Nahon and I. Powis, *Rev. Sci. Instrum.*, 2004, **75**, 4989.
29 H.-J. Werner, P. J. Knowles, G. Knizia, F. R. Manby, M. Schutz and et al., *MOLPRO, version 2012.1, a package of ab initio programs*, 2012.
30 P. J. Knowles and H.-J.Werner, *Chem. Phys. Lett.*, 1985, **115**, 259.
31 J. Heinze, N. Heberle and K. Kohse-Hoinghaus, *Chem. Phys. Lett.*, 1994, **223**, 305.
32 H.-J.Werner, *Mol. Phys.*, 1996, **89**, 645.
33 R. A. Kendall, T. H. Dunning and R. J. Harrison, *J. Chem. Phys.*, 1992, **96**, 6796.
34 H.-J.Werner and P. J. Knowles, *J. Chem. Phys.*, 1988, **89**, 5803.
35 R. O. Loo, H. P. Haerri, G. E. Hall and P. L. Houston, *J. Chem. Phys.*, 1989, **90**, 4222.
36 *National Institute of Standards and Technology, NIST Chemistry Webbook*, 2010, **http://webbook.nist.gov**,.
37 C. D. Sherrill, T. J. V. Huis, Y. Yamaguchi and H. F. S. III, *J. Molec. Struct. (THEOCHEM)*, 1997, **400**, 139.
38 A. García-Vela, *J. Phys. Chem. A*, 2014, **118**, 6395.